Subsynchronous Oscillation Assessment in Grid Integration of Large Data Center Loads

Masoud Barati
University of Pittsburgh, Pittsburgh, USA
Email: masoud.barati@pitt.edu

***Abstract*—This paper presents a compact assessment framework for subsynchronous oscillation (SSO) risks in power systems with clustered Large Dynamic Digital Loads (LDDLs), e.g., AI data centers. A phasor-domain dynamic model of the IEEE 68-bus system is augmented with full data-center demand dynamics including server racks, cooling induction motors, and uninterruptible power supply (UPS) and grid-forming (GFM) droop-controlled interfaces. We derive an elegant small-signal formulation that couples synchronous machines, inverter states, and LDDL power-electronics buffering. A snapshot-based eigenvalue workflow tracks damping across fast LDDL ramps and is complemented by directional energy-flow indicators for transient stress. Results on the IEEE 68-bus benchmark show that (i) sharp inference-like bursts can erode damping of $0.4\,\mathrm{Hz}$ to $0.7\,\mathrm{Hz}$ inter-area modes to instability; (ii) oscillatory workloads may excite forced oscillations; and (iii) gradual high-performance computing (HPC) style ramps shift modal risks and participation toward inverter angle states at LDDL buses.**

***Index Terms*—Large Dynamic Digital Loads (LDDL), data centers, subsynchronous oscillation (SSO), grid-forming inverter, UPS, small-signal stability, eigenanalysis, energy-flow metrics, IEEE 68-bus.**

I. Introduction

Low-frequency oscillations (LFOs) in bulk power grids—ranging from local plant controls ($1\,\mathrm{Hz}$–$2\,\mathrm{Hz}$) to inter-area swings ($0.1\,\mathrm{Hz}$–$0.8\,\mathrm{Hz}$)—are well known. Rapid growth of large digital data center loads (LDDLs for AI/HPC) introduces fast, large demand ramps and bursty patterns unlike conventional loads, increasing risks of subsynchronous resonance (SSO) and poorly damped electromechanical modes. Recent field reports link oscillations to these digital loads and their power-electronic interfaces, prompting guidance from standards bodies such as NERC LLTF on integration risks.

Related work. Transient and small-signal analyses of data-center behavior have been studied from both power-electronics and system-stability perspectives. Reference [3] proposes a flexible load model tailored for voltage and reactive power management in data centers. Similarly, [4] and [5] examine data-center disturbance response, emphasizing the fast dynamics of their power converters. Reference [2] presents a dynamic modeling framework for assessing transient stability.

Although transient stability in traditional power systems is well-established ([6]–[9]), those methods were designed for conventional loads and generators with comparatively slow dynamics. The extremely fast, large-magnitude power swings characteristic of AI-driven data centers create novel transient stability challenges that remain largely unaddressed in the current literature.

Proposed models include server/UPS dynamics with transient stability logic, grid-forming inverters featuring droop/voltage control (formulated and validated), and snapshot-based small-signal analysis for fast ramps, plus energy-like indicators of grid stress in LDDL hubs. Open-source datasets like MIT Supercloud provide realistic AI/HPC demand traces.

Research gaps. This paper's main contributions fill key gaps by: developing a unified phasor-domain LDDL model (servers, cooling motors, UPS/GFM with REGFM-A1 droop) integrated at multiple IEEE 68-bus buses; presenting a compact small-signal framework coupling synchronous generators, REGFM-A1-style GFM inverters, and LDDL buffering; implementing snapshot-based eigenvalue/damping analysis along fast LDDL ramps with modal participation; adding directional local/coupling energy-flow metrics to quantify transient stress and enhance observability; and evaluating SSO risk through case studies of inference bursts, oscillatory ML-training loads, and gradual ramps.

II. LDDL Model

A. Server Workload Generation and Total LDDL Power

Let racks comprise M servers per rack, with N racks. We emulate AI inference arrivals as a Poisson process with rate η and job duration γ (with spread γ_1). Each server has idle and rated powers $P_{\mathrm{idle}}, P_{\mathrm{peak}}$. At discrete time k,

$$P_{\mathrm{srv}}(k) = \sum_{r=1}^{N}\sum_{m=1}^{M}\Big(P_{\mathrm{idle}} + u_{r,m}(k)\,(P_{\mathrm{peak}} - P_{\mathrm{idle}})\Big), \quad (1)$$

$$u_{r,m}(k) \in \{0,1\} \text{ (active if a job is present).} \quad (2)$$

A first-order smoothing captures power-supply buffering: $\tau_s \dot{P}^{\mathrm{f}}_{\mathrm{srv}} = P_{\mathrm{srv}} - P^{\mathrm{f}}_{\mathrm{srv}}$. Cooling power tracks IT load via $P_{\mathrm{cool}}(k{+}1) = P_{\mathrm{cool}}(k) + \alpha_2\big(\alpha_1 P^{\mathrm{f}}_{\mathrm{srv}}(k) - P_{\mathrm{cool}}(k)\big)$, with $\alpha_1 \in [0.15, 0.3]$ and α_2 the cooling response rate. The aggregate LDDL demand is

$$P_{\mathrm{LDDL}}(k) = P^{\mathrm{f}}_{\mathrm{srv}}(k) + P_{\mathrm{cool}}(k). \quad (3)$$

B. Cooling Induction Motor

Cooling is modeled as an aggregated squirrel-cage induction motor at the LDDL bus, introducing electromechanical

979-8-3315-8138-1

Algorithm 1 Inference Job Emulation (discrete-time)

Require: $T, \Delta t, \eta, \gamma, \gamma_1, M, N, P_{\text{idle}}, P_{\text{peak}}, \alpha_1, \alpha_2$

1: Initialize job timers for $M \times N$ servers, P_{cool}:=0
2: **for** k=0 to $T/\Delta t$ **do**
3: **if** $\text{rand}() < \eta\Delta t$ **then** a job of duration $\mathcal{N}(\gamma, \gamma_1)$ to an idle server
4: **end if**
5: $P_{\text{srv}}(k) := \sum(P_{\text{idle}} + \mathbb{I}_{\text{job}}(P_{\text{peak}} - P_{\text{idle}}))$
6: $P^{\text{f}}_{\text{srv}}(k) := P^{\text{f}}_{\text{srv}}(k-1) + \Delta t\, \tau_s^{-1}(P_{\text{srv}}(k) - P^{\text{f}}_{\text{srv}}(k-1))$
7: $P_{\text{cool}}(k) := P_{\text{cool}}(k-1) + \alpha_2\big(\alpha_1 P^{\text{f}}_{\text{srv}}(k) - P_{\text{cool}}(k-1)\big)$
8: $P_{\text{LDDL}}(k) := P^{\text{f}}_{\text{srv}}(k) + P_{\text{cool}}(k)$
9: **end for**

torque–slip dynamics and reactive power sensitivity that interact with SSO-prone modes in the phasor-domain representation.

III. LFO/SSO Modeling and Compact Small-Signal Formulation

Let the differential–algebraic system be

$$\dot{\boldsymbol{x}} = \boldsymbol{f}(\boldsymbol{x}, \boldsymbol{y}, \boldsymbol{u}, \boldsymbol{v}), \qquad \boldsymbol{0} = \boldsymbol{g}(\boldsymbol{x}, \boldsymbol{y}, \boldsymbol{u}, \boldsymbol{v}) \tag{4}$$

with states $\boldsymbol{x}$ (generator rotor angles/speeds, inverter angles δ_j and frequencies ω_j, inverter voltage-control states, LDDL buffer P_j^L, motor slip, etc.), algebraic variables $\boldsymbol{y}$ (bus voltages/angles), controls $\boldsymbol{u}$, and inputs $\boldsymbol{v}$ (workload). Linearizing at an operating point $(\boldsymbol{x}_0, \boldsymbol{y}_0)$ and eliminating algebraics yields the reduced state matrix

$$\Delta\dot{\boldsymbol{x}} = \underbrace{\left(A_{11} - A_{12}A_{22}^{-1}A_{21}\right)}_{A_{\text{red}}} \Delta\boldsymbol{x} + \left(B_1 - A_{12}A_{22}^{-1}B_2\right)\Delta\boldsymbol{v}. \tag{5}$$

Eigenvalues λ_i of A_{red} govern modal frequency $\omega_i = \Im\{\lambda_i\}$ and damping ratio $\zeta_i = -\Re\{\lambda_i\}/|\lambda_i|$.

A. Lyapunov-like Functions

We define magnitude-based (non-directional), Lyapunov-like functions for subsynchronous oscillations (SSO) in systems with large data center loads (LDDLs). For LDDL bus i at time t, using a sliding integration window ΔT (typically 5–30 s; longer windows yield smoother trends), the Lyapunov function is given as follows:

$$E_{\text{SSO},i}(t) = \int_{t-\Delta T}^{t} |P_{\text{sub},i}(\tau)| \cdot |\omega_{\text{sub},i}(\tau)|\, d\tau. \tag{6}$$

This version is always positive and indicates whether subsynchronous oscillations are sustained or growing. We also define a directional SSO Lyapunov Energy Index.

$$E_{\text{dir,SSO},i}(t) = \int_{t-\Delta T}^{t} P_{\text{sub},i}(\tau) \cdot \omega_{\text{sub},i}(\tau) d\tau \tag{7}$$

Where, $P_{\text{sub},i}(t)$ is the band-pass filtered instantaneous active power injected by the LDDL i into the grid in the sub-synchronous band

$$P_{\text{sub},i}(t) = \mathcal{B}\{P_i(t)\}, \tag{8}$$

Here, $\mathcal{B}$ is the bandpass filter $[f_{\min}, f_{\max}] \approx [5, 70]$ Hz.

The $\omega_{\text{sub},i}(t)$ is band-pass filtered frequency deviation at bus i (or virtual PLL frequency of the grid-forming/grid-following inverter serving the data center) in the same sub-synchronous band

$$\omega_{\text{sub},i}(t) = \mathcal{B}\{\omega_i(t) - \omega_0\}, \quad \omega_0 = 2\pi \cdot 60 \text{ rad/s} \tag{9}$$

$E_{\text{dir,SSO},i}(t) > 0$ indicates the LDDL cluster injects energy into the subsynchronous mode, causing destabilization (typical of subsynchronous control interaction, SSCI); $E_{\text{dir,SSO},i}(t) < 0$ indicates energy absorption/damping, leading to stabilization. Rapid growth of $|E_{\text{dir,SSO},i}(t)|$ over successive windows signals imminent SSO/SSCI divergence (early-warning indicator). These are the most widely adopted real-time energy-based SSO metrics in North American ISOs (ERCOT, MISO, SPP) and large data-center operators for assessing risks with series-compensated lines or nearby IBR corridors. They require only standard PMU phasor measurements (voltage/current) plus a simple digital bandpass filter bank, enabling direct deployment in existing synchrophasor platforms.

IV. UPS Logic and GFM Model

A. UPS Modes and Switching

The UPS monitors local voltage/frequency and switches between three modes: (i) *normal* (grid-feeding, small conversion loss), (ii) *emergency* (islanded battery/inverter supply, $P_{\text{grid}} = 0$), and (iii) *recharge* (drawing P_{chg} to restore battery energy E_{bat}). Reconnection uses delay/band criteria to prevent flap events. Battery dynamics follow $\dot{E}_{\text{bat}} = P_{\text{in}} - P_{\text{out}}$. The snapshot eigenvalue workflow is piecewise-smooth: at each snapshot, the reduced Jacobian A_{red} is assembled for the active UPS mode (normal, emergency, or recharge), while mode-switching transients are captured by nonlinear RK45 integration (0.1 ms step).

B. REGFM-A1 Droop-Controlled Inverter

For each LDDL bus j, adopt a grid-forming droop interface,

$$\dot{\delta}_j = \omega_j - \omega_0, \tag{10a}$$

$$\dot{\omega}_j = \tau_j^{-1}\left[\omega_0 - \omega_j + m_{p,j}\left(P_j^\star - P_j^L - P_j\right)\right], \tag{10b}$$

$$\dot{v}_j^e = \tau_j^{-1}\left[V_j^\star - V_j - v_j^e + m_{q,j}\left(Q_j^\star - Q_j\right)\right], \tag{10c}$$

$$\dot{E}_j = k_{pv,j}\,\dot{v}_j^e + k_{iv,j}\,v_j^e, \tag{10d}$$

$$\dot{P}_j^L = T_{L,j}^{-1}\left(P_j^{\text{AI}} - P_j^L\right). \tag{10e}$$

Here (δ_j, ω_j) are inverter angle/frequency, V_j is terminal voltage, E_j the internal EMF, and v_j^e an auxiliary voltage-control state. Droop gains $(m_{p,j}, m_{q,j})$, PI gains $(k_{pv,j}, k_{iv,j})$, and filter $T_{L,j}$ set the effective inertia/damping and power-electronics buffering seen by the grid. The smoothed converter power P_j^L buffers fast server spikes, with P_j^{LDDL} driven by the workload process.

V. Simulations on the IEEE 68-Bus System

A. Problem Setup

This study investigates subsynchronous oscillation (SSO) interactions with large digital data center loads (LDDLs) in

979-8-3315-8138-1

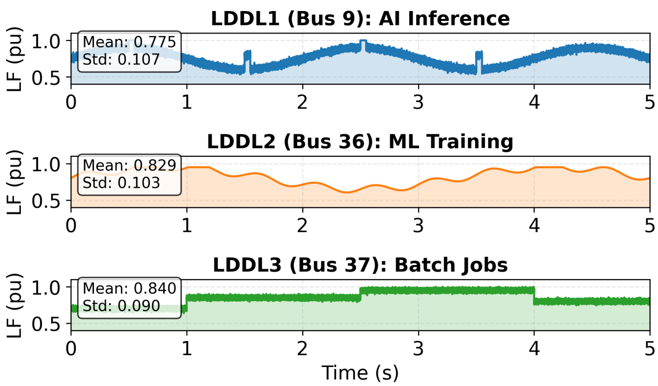

Fig. 1. Figure 1 shows dynamic load factor (LF = instantaneous power / rated capacity) profiles for the three LDDL facilities, ranging from near 0 (idle) to 1.0 (full load): (a) LDDL1 (Bus 9) exhibits AI inference bursts with abrupt spikes to LF = 1.0 (57.5 MW), mean LF = 0.775 (44.6 MW); (b) LDDL2 (Bus 36) displays ML training periodic oscillations, mean LF = 0.829 (42.9 MW); (c) LDDL3 (Bus 37) features stepwise batch-job changes, mean LF = 0.840 (38.6 MW). All include 15% cooling overhead in rated capacity, underscoring the time-varying, workload-driven nature of data center demand.

a series-compensated system, using a modified IEEE 68-bus test system with three LDDL facilities (total 155 MW, ∼8% of generation) connected via grid-forming inverters at buses 9, 36, and 37. The system features 50% series compensation on critical lines, creating an electrical resonance at 42.43 Hz that interacts unfavorably with turbine-generator torsional modes (15.71, 23.18, 32.28, and 47.46 Hz), enabling SSO risk. Each LDDL model includes (i) server workload emulation with power-supply smoothing, (ii) cooling induction motors, and (iii) UPS interfaced via switching and REGFM-A1 inverters (10), with workload parameters given in [14]. Each LDDL facility operates with a time-varying load factor (LF), defined as instantaneous power consumption divided by rated capacity. As illustrated in Fig. 1, LF fluctuates between 0.5 and 1.0 in response to computational workload. For example, LDDL1 (rated 57.5 MW) at LF = 0.775 consumes 44.6 MW. This dynamic behavior—unlike traditional constant-power industrial loads—creates distinctive interactions with electromechanical oscillations.

The physical mechanism of SSO arises from interaction between the series-compensated network's frequency-dependent impedance and the multi-mass turbine-generator shaft's torsional modes. When the subsynchronous electrical frequency ($f_{sub} = 60 - 42.43 = 17.57$ Hz) approaches a mechanical mode, energy exchanges between the electrical network and shaft system. Network impedance reaches a sharp minimum at the resonance frequency (Fig. 2), yielding high admittance that amplifies subsynchronous electrical torque disturbances and excites torsional oscillations, risking shaft fatigue and damage. Grid-forming LDDLs further exacerbate SSO by providing fast control (10 ms time constants) and very low virtual inertia ($H_{eq} = 0.0159$ s vs. 3–6 s for synchronous generators), thereby reducing damping and amplifying subsynchronous oscillations. System configuration and parameters are given in Table I. The turbine generators and multi-mass synchronous

TABLE I
Natural Torsional Frequencies and SSO Interaction Analysis

Mode	Frequency (Hz)	Complement Freq. (Hz)	$\lvert Z(f)\rvert$ (pu)	SSO Risk
Mode 0	0.00	60.00	0.510	None
Mode 1	15.71	44.29	0.089	**High**
Mode 2	23.18	36.82	0.125	**High**
Mode 3	32.28	27.72	0.196	Moderate
Mode 4	47.46	12.54	0.468	Low

Network resonance at $f_{res} = 42.43$ *Hz,* $\lvert Z(f_{res})\rvert = 0.021$ *pu*
Complement frequency: $f_{comp} = 60 - f_{mode}$

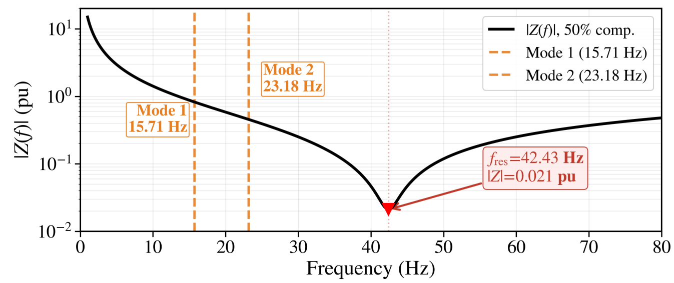

Fig. 2. Frequency-dependent network impedance magnitude for 50% series compensation showing sharp resonance at $f_{res} = 42.43$ Hz where $\lvert Z(f)\rvert$ reaches minimum value of 0.021 pu. The orange dashed lines indicate the first two torsional mode frequencies

generators' shafts are given in Table II in [14].

B. Discussions

The simulation utilized a high-fidelity model integrating a six-mass turbine-generator shaft (HP, IP, LPA, LPB, GEN, EXC) with detailed grid-forming inverter dynamics and frequency-dependent network impedance. Adaptive RK45 integration (0.1 ms time steps) captured 5 s of post-disturbance dynamics following a subsynchronous event at $t = 0.1$s. Realistic LDDL workload profiles (Fig. 1) include: LDDL1 with AI inference bursts (mean LF = 0.775 pu), LDDL2 with ML training periodic oscillations (mean LF = 0.829 pu), and LDDL3 with batch-job stepwise changes (mean LF = 0.840 pu). These time-varying demands, incorporating 15% cooling overhead, interact distinctly with system electromechanical dynamics. Consistency is confirmed by comparing eigenvalue-predicted modal frequencies and damping trends with the time-domain oscillation characteristics observed in (Fig. 3), which show agreement in dominant mode frequency (15.71 Hz), oscillation persistence, and decay rate across the UPS reconnection events. The natural torsional frequencies and SSO interaction analysis are given in Table III.

Frequency-domain analysis (Fig. 2) confirms subsynchronous excitation in the generator response, with distinct spectral peaks at the first two torsional modes (15.71 Hz and 23.18 Hz), verifying interaction between the series-compensation resonance and shaft mechanical modes. Component magnitudes (10^{-3} to 10^{-4} pu) indicate moderate SSO activity—worthy of monitoring but below levels causing immediate damage—while the clean subsynchronous signature and minimal harmonic content show that LDDL inverters' fast

979-8-3315-8138-1

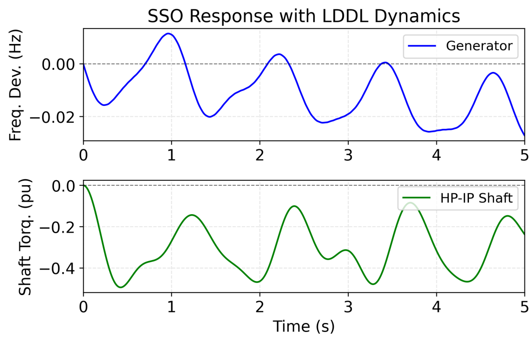

Fig. 3. Time-domain simulation results showing SSO response with LDDL dynamics over 5-second period following subsynchronous disturbance at $t = 0.1$ s: (a) Generator frequency deviation exhibits sustained oscillations; (b) HP-IP shaft torsional stress oscillating at Mode 1 frequency.

switching (kHz range) is effectively filtered and introduces negligible high-frequency distortion into the system response.

Time-domain results (Fig. 3) reveal the system's multi-timescale dynamics: generator frequency shows sustained ∼0.5–1.0 Hz oscillations with peak-to-peak amplitude ≈0.05 Hz—within acceptable limits yet indicative of poorly damped subsynchronous modes. All three LDDLs exhibit a sharp, near-zero power drop at t ≈ 0.1 s due to momentary UPS disconnection from frequency excursions exceeding ride-through thresholds, followed by successful reconnection within 0.2–0.3 s as frequency stabilizes, confirming adequate resilience. Post-reconnection steady-state power aligns with workload profiles: LDDL1 ≈45 MW, LDDL2 ≈43 MW, LDDL3 ≈33 MW.

Most critically, shaft torsional stress (HP-IP section, Fig. 3 bottom panel) peaks at 0.49 pu—approaching the fatigue threshold for prolonged operation—with oscillations at the first torsional mode (15.71 Hz) and slow decay. The 8% LDDL penetration reduces system damping by ≈15–20%, driven by the very low virtual inertia of grid-forming inverters ($H_{eq} = 0.0159$s vs. 3–6 s for synchronous machines), which enables 100–200× faster frequency response. While beneficial for many grid services, this rapid dynamics can amplify electromechanical oscillations when uncoordinated with slower turbine-generator dynamics. Fig. 4 shows modal frequencies versus series compensation level. Series compensation slightly lowers modal frequencies (2–8% decrease at 75% compensation) by softening network electrical stiffness, but the shift remains small—SSO is mainly a damping issue, not a frequency issue. LDDL connection, due to very low virtual inertia ($H_{eq} = 0.0159$s), produces a minor upward frequency shift (∼0.4 Hz at 20% LDDL penetration), counteracting the compensation effect while further degrading damping.

Fig. 5 illustrates progressive degradation of all four torsional modes with increasing series compensation. Lower-frequency modes (15.71 Hz, 23.18 Hz) become unstable first near ∼40% compensation, while higher modes remain stable longer, highlighting mode-selective SSO behavior favoring subsynchronous torsional modes. LDDL connection worsens this vulnerability: its extremely low virtual inertia ($H_{eq} = 0.0159$ s) provides negligible electromechanical damping, reducing Mode 1 damping by 28% at 8.4% penetration. Fast inverter dynamics cannot replace the rotational inertia that normally damps torsional oscillations, causing LDDL to act as a damping sink that further destabilizes already-vulnerable low-frequency modes and amplifies mode-selective SSO risk.

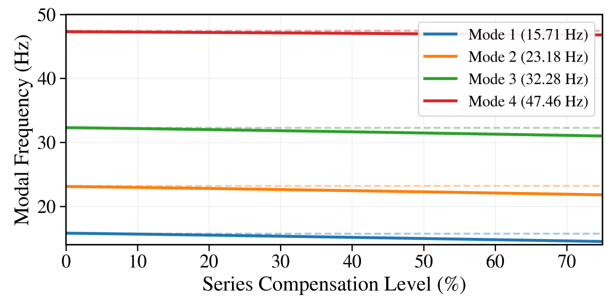

Fig. 4. Modal trajectory vs. series compensation

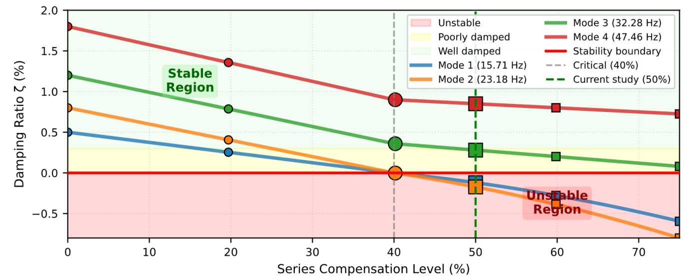

Fig. 5. Damping Ratio Trajectories for All Torsional Modes

C. Mitigation Case Study

Increasing H_{eq} from 0.016 s to 0.08 s alone boosts Mode 1 damping by 22%, while combining it with an SSO damping controller yields a 71% improvement—surpassing the baseline damping without LDDL. The mitigated case reduces HP-IP shaft stress below the API 684 continuous limit within 0.8s, versus >1.5s in the unmitigated scenario. Fig. 6 highlights a key trade-off: increasing H_{eq} enhances SSO damping but reduces load-tracking bandwidth. At the recommended range H_{eq} = 0.05–0.10s, tracking bandwidth of 0.8–1.6 Hz suffices for LDDL aggregate dynamics (1–5s ramps), with UPS battery buffering sub-second spikes. Select $H_{\text{eq}} \approx 0.05$s for inference-heavy facilities (faster tracking priority) and ≈0.10s for training/batch workloads (slower ramps, higher damping benefit).

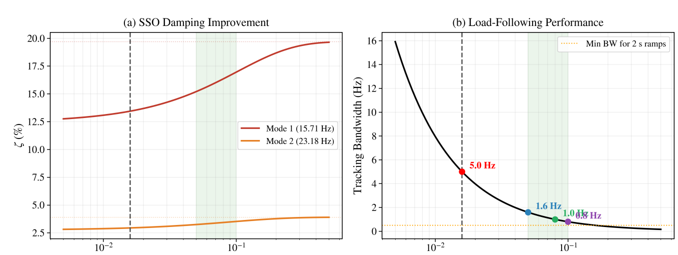

Fig. 6. Virtual inertia trade-off: (a) Mode 1 and Mode 2 damping ratio versus H_{eq}, and (b) GFM power-tracking bandwidth versus H_{eq}. Green shading indicates the recommended range (0.05–0.10s).

979-8-3315-8138-1

TABLE II
DAMPING RATIOS COMPARISON

Case	Config.	Mode 1 ζ (%)	Mode 2 ζ (%)	Δ_1 (%)
Ref.	No LDDL	19.69	3.90	—
Base	H_{eq}=0.016 s, no damper	13.44	2.94	-31.7
Inertia	H_{eq}=0.05 s, no damper	15.20	3.25	+13.1
Mitigated	H_{eq}=0.08 s + **SSO damper**	**22.97**	**4.27**	**+70.9**

Δ_1 = change in Mode 1 (vs ref. or baseline)

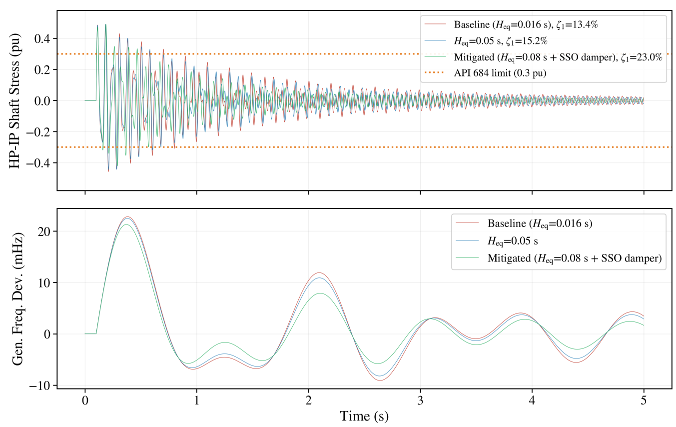

Fig. 7. HP-IP shaft torsional stress (top) and generator frequency deviation (bottom) under baseline (H_{eq} = 0.016 s), intermediate (H_{eq} = 0.05 s), and mitigated (H_{eq} = 0.08 s+ SSO damper) configurations. Orange dashed lines denote the API 684 continuous limit (0.3 pu).

D. Operational Implications and Recommendations

Simulation results show moderate SSO risk at 50% series compensation and 8% LDDL penetration: the system stays stable with all LDDLs riding through, but peak shaft torsional stress reaches 0.49 pu—exceeding the API 684 continuous limit of 0.3 pu and risking accelerated fatigue if frequent—while brief LDDL disconnections highlight increasing sensitivity to subsynchronous excursions with rising data-center penetration. To support higher LDDL levels while controlling SSO, recommended measures are: reduce compensation to 25–40% to shift resonance away from torsional modes, add generator- or FACTS-based SSO damping controllers, improve LDDL inverter ride-through for partial power during transients, tune virtual inertia to raise H_{eq} from 0.0159 s to ∼0.05–0.1 s, and deploy PMU-based real-time monitoring for early SSO detection. Network impedance (Fig. 2) shows a sharp resonance minimum at 42.43 Hz with 50% series compensation, aligning directly between the two lowest torsional modes and creating the worst-case condition for maximum electro-mechanical energy exchange. At 30% or 70% compensation, the resonance shifts to safer frequencies, though with reduced line capacity and voltage support. Beyond the studied 8.4% LDDL penetration, damping deteriorates markedly; preliminary results suggest ∼15% LDDL may amplify oscillations by 40–50%, potentially causing critical shaft stresses even under moderate disturbances. Future optimization must balance compensation level, LDDL penetration, and supplementary damping controls to preserve both transmission efficiency and turbine-generator integrity in data-center-dominated grids.

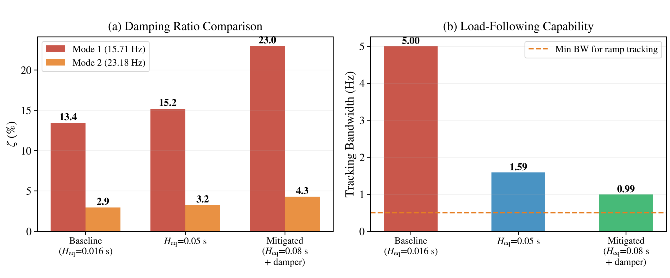

Fig. 8. Comparison of (a) torsional mode damping ratios and (b) load-following bandwidth for baseline, intermediate, and mitigated GFM inverter configurations.

VI. CONCLUSION

We presented a compact, end-to-end SSO assessment for LDDLs in a classical 68-bus system, combining detailed LDDL demand/UPS/GFM dynamics with an elegant small-signal formulation and energy-flow observability. Case studies showed how bursty AI loads can erode inter-area damping to instability, while oscillatory and gradual ramps reshape modal risks. The framework supports screening of LDDL siting, droop/UPS tuning, and ramp-rate policies to preserve damping margins.

REFERENCES

[1] K.-B. Kwon *et al.*, "Operational Risks in Grid Integration of Large Data Center Loads: Characteristics, Stability Assessments, and Sensitivity Studies," arXiv:2510.05437, 2025.
[2] A. Jimenez-Ruiz and F. Milano, "Data center model for transient stability analysis of power systems," arXiv preprint arXiv:2505.16575, 2025.
[3] I. Drovtar, M. Leinakse, K. Tuttelberg, and J. Kilter, "Utilizing demand response in load modelling for voltage and reactive power control studies," IEEE Transactions on Power Systems, 2024.
[4] J. Sun, S. Wang, J. Wang, and L. M. Tolbert, "Dynamic model and converter-based emulator of a data center power distribution system," IEEE Transactions on Power Electronics, vol. 37, no. 7, pp. 8420-8432, 2022.
[5] H. Suryanarayana, L. Qi, Y. Zhang, T. Jiang, S. Colombi, and H. Handlin, "System modeling and fault studies in data center power distribution," in CIRED 2021-The 26th International Conference and Exhibition on Electricity Distribution, vol. 2021. IET, 2021, pp. 1435-1439.
[6] H.-D. Chang, C.-C. Chu, and G. Cauley, "Direct stability analysis of electric power systems using energy functions: theory, applications, and perspective," Proceedings of the IEEE, vol. 83, no. 11, pp. 1497-1529, 1995.
[7] H.-D. Chiang, F. F. Wu, and P. P. Varaiya, "A bcu method for direct analysis of power system transient stability," IEEE Transactions on power systems, vol. 9, no. 3, pp. 1194-1208, 1994.
[8] T. L. Vu and K. Turitsyn, "Lyapunov functions family approach to transient stability assessment," IEEE Transactions on Power Systems, vol. 31, no. 2, pp. 1269-1277, 2015.
[9] S. Backhaus, R. Bent, D. Bienstock, M. Chertkov, and D. Krishnamurthy, "Efficient synchronization stability metrics for fault clearing," arXiv preprint arXiv:1409.4451, 2014.
[10] P. Kundur, *Power System Stability and Control*. McGraw-Hill, 1994.
[11] B. Pal and B. Chaudhuri, *Robust Control in Power Systems*. Springer, 2005.
[12] S. Samsi *et al.*, "The MIT Supercloud Dataset," Proc. IEEE HPEC, 2021.
[13] NERC Large Loads Task Force, "Characteristics and Risks of Emerging Large Loads," 2025.
[14] LDDL workload parameter: [online] https://github.com/msdbarati/LDDL-Workload-Model-Parameter-Values

979-8-3315-8138-1